

Does the Hydroperoxo Species of Cytochrome P450 Participate in Olefin Epoxidation with the Main Oxidant, Compound I? Criticism from Density Functional Theory Calculations

Takashi Kamachi, Yoshihito Shiota, Takehiro Ohta,† and Kazunari Yoshizawa*

Institute for Fundamental Research of Organic Chemistry, Kyushu University, Fukuoka 812-8581

†Center for Integrative Bioscience, Okazaki National Research Institutes, Okazaki 444-8585

(Received December 25, 2001)

Ethylene epoxidation by an iron(III)-hydroperoxo model of cytochrome P450 $Fe(OOH)(C_{20}N_4H_{12})(SCH_3)$ is investigated with the B3LYP density functional theory (DFT) method to look at whether or not the iron(III)–hydroperoxo species can participate in olefin epoxidation with the iron(IV)–oxo species (compound I). The answer is negative. There are two possible entrance channels in the epoxidation reaction, a proximal oxygen transfer mechanism and a distal oxygen transfer mechanism, both mechanisms being stepwise processes involving radical intermediates. In the proximal oxygen transfer mechanism, the homolytic cleavage of the Fe–O bond of the iron(III)–hydroperoxo species initially occurs with a change in the Fe atomic charge from +3 to +2. The proximal oxygen transfer mechanism involves an energetically less stable radical $^{\bullet}CH_2CH_2(OOH)$. In contrast, in the initial stages of the distal oxygen transfer mechanism, the O–O bond of the hydroperoxo ligand is homolytically cleaved, and the iron(IV)–oxo complex thus formed retains a weak interaction with the hydroxy group of the resultant radical intermediate involving $^{\bullet}CH_2CH_2(OH)$. This mechanism is more realistic, but the activation energy of the transition state of the O–O bond cleavage is comparable to that of the corresponding transition state by hydrogen peroxide. The present result suggests that the mechanism and energetics of ethylene epoxidation remain unchanged by the involvement of the iron–porphyrin complex. The epoxidation of ethylene by a compound I model is also calculated to increase our understanding of olefin epoxidation by P450. The mechanism and energetics of olefin epoxidation by iron(III)–hydroperoxo species are less plausible than epoxidation by compound I.

Olefin epoxidation by cytochrome P450 is a crucial biocatalytic process by which nearly all living species can metabolize toxic and endogenous compounds.[1] The catalytically active oxygen species that enables the transfer of an oxygen atom into olefinic substrates is commonly believed to be the high-valent iron–oxo adduct of protoporphyrin IX unit, here called compound I. Extensive experimental as well as theoretical investigations have characterized the important enzymatic functions of this species.[2–22] A widely-believed dioxygen activation process by P450 is shown in Scheme 1, in which iron(III)–peroxo and iron(III)–hydroperoxo species occur before the formation of the iron(IV)–oxo species. The conversion of iron–peroxo species to iron–hydroperoxo species is promoted by the proton delivery system that consists of amino acid residues and solvent water. Uptake of a second proton by the iron(III)–hydroperoxo species would then lead irreversibly to the iron(IV)–oxo species. These unstable species in the catalytic cycle of P450cam were tentatively identified by Schlichting and collaborators using transient state crystallographic techniques.[23] Loew and Harris carried out density functional theory (DFT) computational studies for this dioxygen activation process and supported this proton-assisted mechanism of the O–O bond cleavage to form compound I.[24]

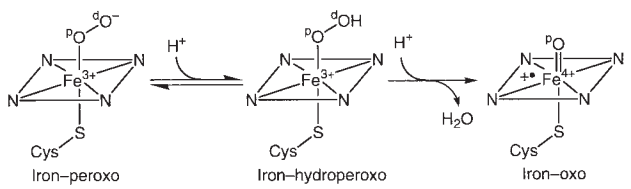

Scheme 1.

Coon and collaborators investigated the reactivity of the mutants of P450s 2B4 and 2E1 in which the threonine, which is believed to facilitate proton delivery to the active site, was replaced by alanine. They suggested that the iron(III)–hydroperoxo species as well as the iron(IV)–oxo species can effect olefin epoxidation.[25] In their mutant study, the reduced proton delivery is believed to interfere with the activation of dioxygen, and thus the lifetime of the iron(III)–hydroperoxo species is elongated to be capable of oxygenating substrates prior to the O–O bond scission. Of particular interest in the reactivity of their mutants is that the T303A mutation of P450 2E1 resulted in the enhancement of olefin epoxidation along with the suppression of allylic hydroxylation of cyclohexene and butene. Nam et al.[26] also suggested the involvement of iron(III)–hydroperoxo species as an active oxidant in various olefin epoxidation reactions. Watanabe, Morishima, and collaborators[27] previously demonstrated that an iron(III)–acylperoxo porphyrin complex directly mediates olefin epoxidation. Valentine and co-workers[28] reported that in-situ generated iron–peroxo porphyrin complexes are powerful nucleophiles capable of epoxidizing electron-deficient olefins. These studies suggest that iron(III)–hydroperoxo as well as iron–peroxo species can mediate olefin epoxidation.

Considering the broad reaction specificity and variety of products formed by P450, many find that the new paradigm of oxygenation where P450 uses several different active oxidants is attractive.[25] It is of particular interest to investigate the reactivity of the various intermediates of P450 to olefins by means of computational quantum chemistry. Shaik and collaborators[29] demonstrated that compound I of P450 reacts with ethylene to form an intermediate complex with a covalent C–O bond and a carbon-centered radical on the closely-lying quartet and doublet potential energy surfaces; the quartet spin intermediate has a substantial barrier for the transformation to the epoxide complex, while the doublet spin intermediate collapses to the epoxide complex with virtually no barrier. To increase our understanding of the enzymatic diversity of P450, we should also characterize the oxygenating ability of the hydroperoxo species to olefins. The purpose of our study is to address the question "Does the iron–hydroperoxo species of P450 participate in olefin epoxidation with the iron–oxo species?" It is useful to determine whether the oxygen atom insertion into a C=C double bond is mediated by the distal oxygen atom (^{d}O) or by the proximal oxygen atom (^{p}O) of the iron(III)–hydroperoxo species. In order to answer these questions, we performed DFT computations with respect to ethylene epoxidation by an iron(III)–hydroperoxo model of P450. The answer is "No".

Model System and Method of Calculation

We adopted a six-coordinate iron–porphyrin complex $Fe^{+3}(OOH)^{-1}(C_{20}N_4H_{12})^{-2}(SCH_3)^{-1}$ as an iron(III)–hydroperoxo model of P450 and ethylene as substrate. Thus, the total charge of the model reacting system is −1. We selected the commonly used CH_3S^- species as an axial ligand model of the actual cysteinate ligand of cytochrome P450. The energies and geometries of the reactants, intermediates, products, and transition states were calculated with the spin-unrestricted version of the B3LYP DFT method,[30] which consists of the Slater exchange, the Hartree–Fock exchange, the exchange functional of Becke,[31] the correlation functional of Lee, Yang, and Parr (LYP),[32] and the correlation functional of Vosko, Wilk, and Nusair.[33] We considered the sextet, quartet, and doublet spin states. In optimizing geometries, we used the compact effective potentials[34] (CEP) of Stevens, Basch, and Krauss with the [8s8p6d/4s4p3d] basis function for Fe and with the 1-2-1 "triple-ζ" basis function (CEP-121G) for S, the 6-31G basis set[35] for the nitrogen atoms of porphyrin, the carbon and hydrogen atoms of ethylene, and the hydroperoxo moiety, and the STO-3G basis set[36] for the rest of the atoms of the porphyrin ring. All the geometries for reaction species and transition states were fully optimized without symmetry constraints. We confirmed from systematic vibrational analyses that each transition state has only one imaginary frequency mode. To confirm the applicability of the mixture of the basis sets, we carried out single-point calculations with the 6-31G(d) basis set for all atoms except Fe and S, as listed in Table 1.[35a,37] These additional calculations support our discussions.[38] We used the Gaussian 98 software package.[39]

Results and Discussion

We found that the iron(III)–hydroperoxo species can mediate ethylene epoxidation via two reaction entrance channels. One mechanism involves the transfer of the proximal oxygen atom to the substrate, followed by the O–O bond cleavage and ring-closure to lead to epoxide. We term it a "proximal oxygen transfer mechanism". The other mechanism is initiated by the O–O bond cleavage and the distal oxygen atom is transferred to the substrate. We term this a "distal oxygen transfer mechanism". Energy diagrams and optimized geometries for these mechanisms are depicted in Figs. 1–3. We demonstrate here that the iron(III)–hydroperoxo species cannot mediate olefin epoxidation because the activation barriers for these mechanisms are rather high.

Table 1. Energies of the Reaction Species of Olefin Epoxidation by Iron-Hydroperoxo and -Oxo Species Determined by Single-Point Calculations (Unit in kcal/mol)

	Doublet	Quartet	Sextet
Iron-hydroperoxo complex	0.0	15.5	9.2
TS1-p	35.4	37.2	—
TS1-d	—	—	32.4
Int-p	30.8	30.9	23.3
Int-d	−5.7	−5.7	1.3
TS2-d	10.5	17.4	—
Final complex	−43.5	−29.2	—
Compound I	—	0.0	—
TS1-com	—	16.1	—
Int-com	—	−1.1	—
TS2-com	—	1.9	—
Product complex	—	−35.2	—
Final complex	—	−31.8	—

For Fe S atoms compact effective potentials, for the rest atoms 6-31G* basis set.

1. Structures of Iron(III)–Hydroperoxo Species. We first studied the electronic structure of the iron(III)–hydroperoxo species to look at whether this transient intermediate can participate in olefin epoxidation or not. In contrast to inorganic Fe^{3+}-containing compounds, ferric porphyrins have close-lying doublet, quartet, and sextet spin states.[40,41] Harris and Loew reported from INDO/S–ROHF/CI calculations that the excitation energies from the doublet state to the quartet and sextet states are 4.9 and 8.4 kcal/mol, respectively, on a peroxidase model that has a neutral imidazole axial ligand.[42] The ground state of our iron(III)–hydroperoxo model with a thiolate axial ligand is a doublet, the sextet (quartet) state lying 5.3 (10.9) kcal/mol above the doublet state. The low-lying doublet and sextet states should be responsible for olefin epoxidation in the initial stages of the reaction if the iron(III)–hydroperoxo species is a real oxidant.

As shown in Fig. 2, the H atom of the OOH ligand faces the porphyrin ring. This structure is enegetically the most stable conformation about the Fe–O–O–H dihedral angle and allows the subsequent protonation that produces compound I easily. The optimized O–O bond distance is 1.540, 1.532, and 1.525 Å in the doublet, quartet, and sextet spin states, respectively, these distances being almost equal to the O–O bond distance (1.531 Å) of hydrogen peroxide at the same level of theory. The Fe–O and Fe–S distances are shorter in the doublet state than in the sextet and quartet states by 0.1 and 0.2 Å, respectively. The change in these bond distances can be explained by the molecular orbital analysis shown in Chart 1. In the sextet and quartet states, the $\sigma^*(d_{z^2})$ orbital, which is out-of-phase (antibonding) along the

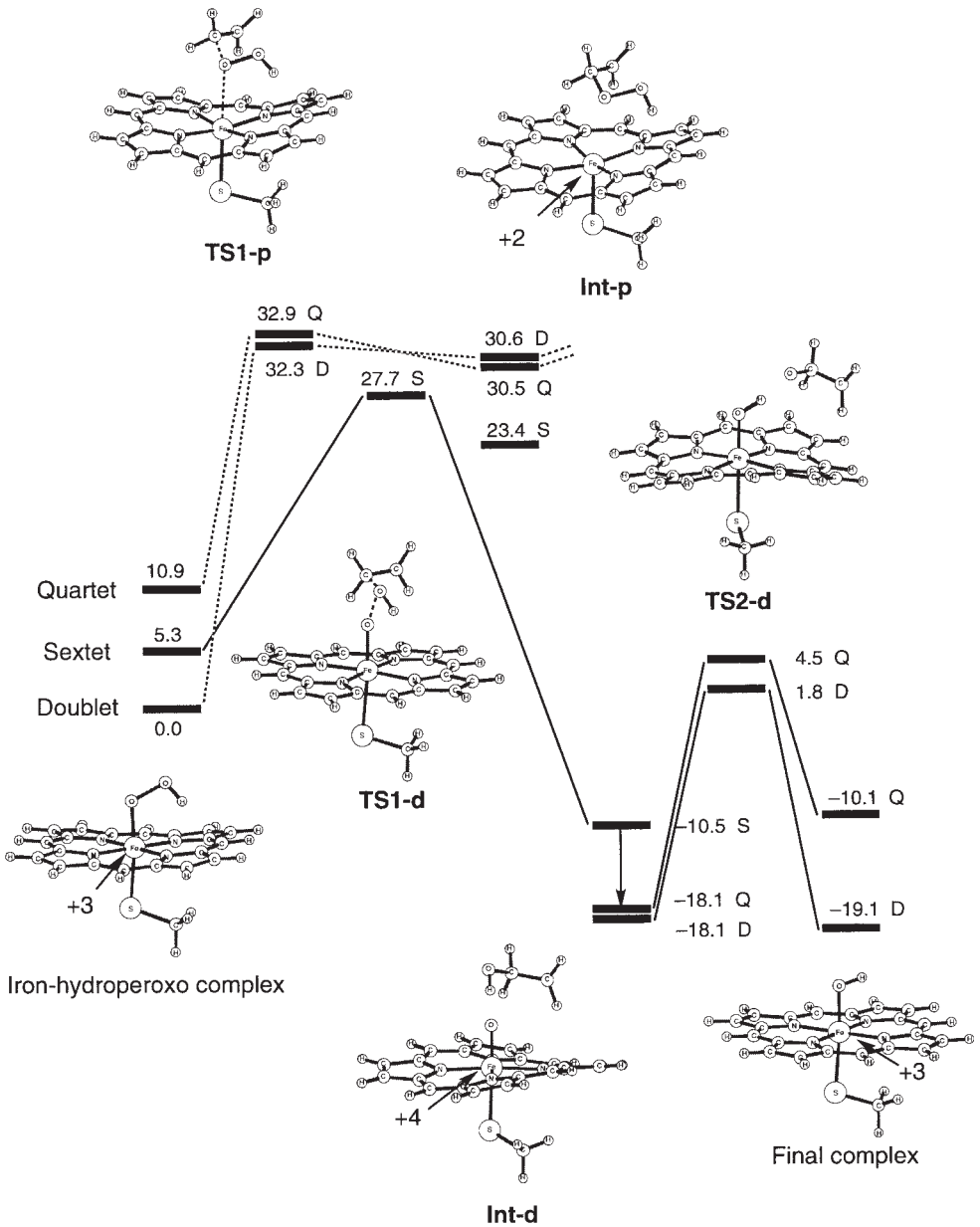

Fig. 1. Energy diagrams for ethylene epoxidation by an iron(Ⅲ)–hydroperoxo species model in the spin doublet, quartet, and sextet states.

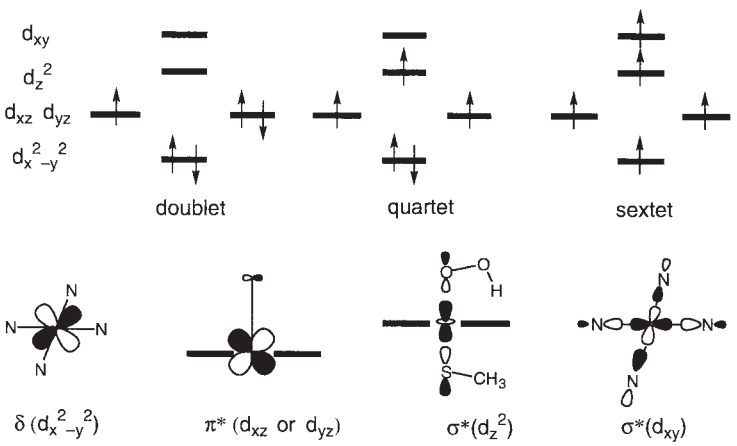

Chart 1.

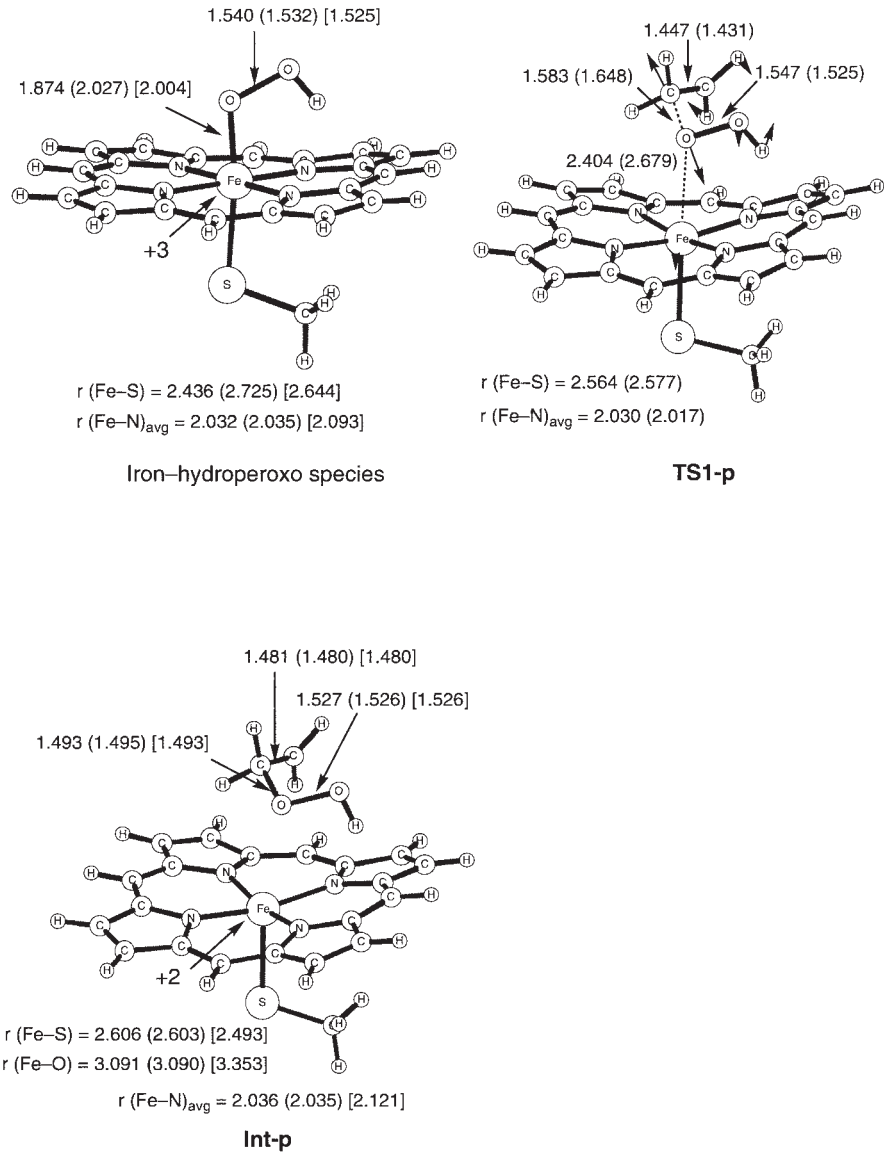

Fig. 2. Optimized geometries and their imaginary mode of reaction species for the proximal oxygen transfer mechanism in the doublet, (quartet), and [sextet] states. Values in units of Å.

S–Fe–O axis, is occupied by one electron. The antibonding interaction results in the elongation of the Fe–O and Fe–S bonds when the orbital is occupied in the sextet and quartet spin states, whereas this orbital is unoccupied in the doublet state. The Fe–N distances in the sextet state are longer than those in the doublet and quartet states because in the sextet state the $\sigma^*(d_{xy})$ orbital, which has an antibonding nature with respect to the Fe–N bonds, is occupied by one electron.

Computed atomic charges and spin densities for the iron(Ⅲ)–hydroperoxo species are listed in Table 2. The spin density of this species is heavily localized on the Fe atom (the porphyrin ring and the thiolate ligand have virtually no spin density).[43] In contrast, the porphyrin and thiolate ligands of compound I have large spin densities because the two ligands are oxidized in the high oxidation state, resulting in a porphyrin π cation radical species or a thiolate radical species.[44–50]

Table 2. Calculated Mulliken Charges and Spin Densities for the Fe and O atoms and the CH_3S and Porphyrin (Por) Moieties of Iron–Hydroperoxo Species (Values in Parentheses are Spin Densities)

	Doublet	Quartet	Sextet
Fe	1.2 (1.0)	1.4 (2.6)	1.4 (4.2)
O (proximal)	−0.4 (0.1)	−0.4 (0.3)	−0.4 (0.3)
O (distal)	−0.5 (0.0)	−0.5 (0.0)	−0.5 (0.0)
H	0.3 (0.0)	0.3 (0.0)	0.3 (0.0)
CH_3S	−0.4 (0.0)	−0.6 (0.2)	−0.5 (0.2)
Por	−1.2 (−0.1)	−1.2 (−0.1)	−1.3 (0.3)

2. Energy Profile for Olefin Epoxidation. Figure 1 shows a computed potential-energy profile for ethylene epoxidation by the iron(Ⅲ)–hydroperoxo species. Let us first consider the transfer of the proximal oxygen atom to the substrate in the reaction entrance. We show in Fig. 2 optimized geometries of the intermediate and transition state involved in the proximal oxygen transfer mechanism. When a carbon atom of ethylene comes into contact

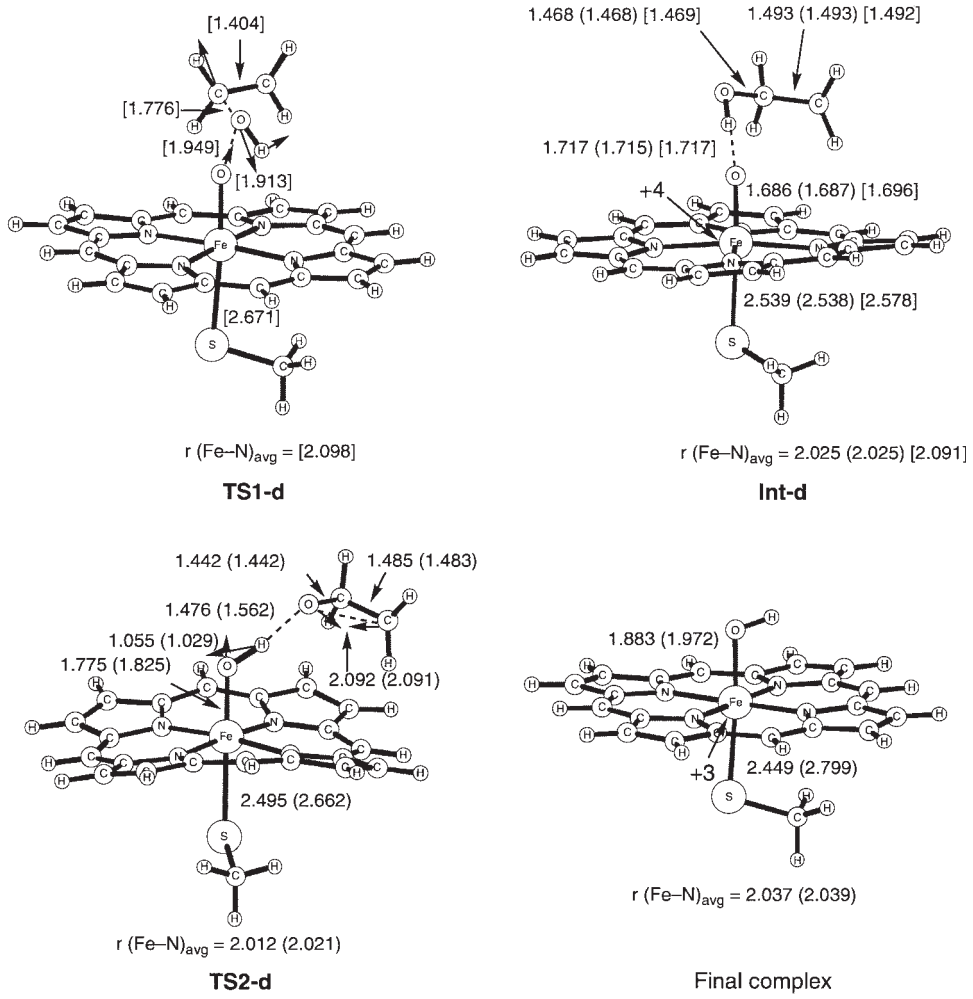

Fig. 3. Optimized geometries and their imaginary mode of reaction species for the distal oxygen transfer mechanism in the doublet, (quartet), and [sextet] states. Values in units of Å.

with the proximal oxygen atom, a weakly-bound intermediate, **Int-p**, is generated via **TS1-p** that involves the cleavage of the Fe–O bond and the formation of the C–O bond. We successfully obtained it in the doublet and quartet states. The barrier height for the proximal oxygen transfer measured from the dissociation limit of the isolated starting materials is 32.3 and 22.0 kcal/mol in the doublet and quartet states, respectively. The activation energy of **TS1-p** depends heavily on the spin state because the migrating proximal oxygen atom is directly bound to the Fe atom and changes the electronic situation of the d-block orbital as the oxidation reaction proceeds. This is confirmed by a drastic change in the spin density of the iron atom from 1.0 (2.6) in the iron(Ⅲ)–hydroperoxo complex to 1.8 (2.4) in **TS1-p** in the doublet (quartet) state. Complex **Int-p** lies more than 30 kcal/mol above **Int-d** that is a radical intermediate being formed in the distal oxygen transfer mechanism, because **Int-p** has a coordinatively unsaturated iron and an unstable hydroperoxo group. Moreover, we considered the O–O bond cleavage pathway that releases hydroxyl radical by the formation of the C–O bond between ethylene and the proximal oxygen. A resultant radical intermediate has relative energies of 32.0 (32.0) [32.8] kcal/mol in the doublet (quartet) [sextet] states and also lies more than 40 kcal/mol above **Int-d**. We therefore conclude that the proximal oxygen transfer mechanism is not a feasible reaction pathway for olefin epoxidation.

On the other hand, in the initial stages of the distal oxygen transfer mechanism the O–O bond of the hydroperoxo moiety is cleaved and the distal oxygen atom is transferred to one of the carbon atoms of ethylene via **TS1-d**. The activation energy for the first transition state **TS1-d** in this mechanism is 22.4 kcal/mol in the sextet state. This is rather high for olefin epoxidation reactions.[51–55] For example, Cavallo et al. computed the epoxidation of ethylene by Mn-salen catalyst, the active center of which is the Mn–O species, and demonstrated that the barrier for the first step amounts to only 12 kJ/mol (2.9 kcal/mol).[56] Moreover, the computed activation energy of 22.4 kcal/mol for **TS1-d** is comparable to that for the transition state by hydrogen peroxide, 22.1 kcal/mol, as discussed below in detail. In the resultant intermediate **Int-d**, the iron(Ⅳ)–oxo species retains a weak interaction with the hydroxy group of the oxidized substrate radical $^{\bullet}CH_2CH_2(OH)$. The energetical closeness between the doublet and quartet states of **Int-d** suggests that the spin coupling between the FeO moiety and the radical center of the oxidized substrate is small. The hydrogen atom abstraction from the O–H bond by the oxo ligand and the ring closure of the C–C–O triangle synchronously occur via **TS2-d**, leading to the formation of

epoxide. We propose here two possible mechanisms for olefin epoxidation by the iron(Ⅲ)–hydroperoxo species "proximal oxygen transfer mechanism" and "distal oxygen transfer mechanism". However, the transition states for the transfer of proximal or distal oxygen have rather high barriers for olefin epoxidation. Thus, the iron(Ⅲ)–hydroperoxo species cannot participate in this reaction.

3. Proximal Oxygen Transfer Mechanism. The reactivity of the •OOH species has been discussed mainly in the fields of catalytic chemistry and atmospheric chemistry from experimental and theoretical points of view.[57–59] Clark and Hofmann studied the mechanism and energetics for the oxidation of methane to methanol and the epoxidation of ethylene by the •OOH species using ab initio molecular orbital calculations,[60] and proposed a mechanism different from the so-called oxygen rebound mechanism of P450-mediated alkane hydroxylation,[1a,h] in which an iron(Ⅳ)–oxo species plays a central role as a hydrogen-abstracting species. According to their proposal, the H atom of methane is abstracted by the oxygen atom that corresponds to the proximal oxygen atom of the iron(Ⅲ)–hydroperoxo speices.

When ethylene approaches the proximal oxygen atom, a covalent bond is formed between the oxygen atom and a carbon atom of ethylene via **TS1-p**. This new bond is responsible for the homolytic cleavage of the Fe–O bond to lead to the release of the •OOH species. **TS1-p** has one imaginary vibrational frequency at 179i and 384i cm^{-1} in the doublet and quartet states, respectively, which is mainly due to Fe–O and C–O stretching. This transition state is thus consistent with the "proximal oxygen transfer mechanism".

We can characterize what is happening in the proximal oxygen transfer mechanism from a simple molecular orbital consideration. We show in Chart 2 the essential molecular orbitals and their occupation in **Int-p**. In the doublet state, the unoccupied d_z^2 orbital of the iron(Ⅲ)–hydroperoxo species (indicated in Chart 1), which has an antibonding character in the Fe–O bond, should accept one electron from the π orbital of ethylene to cleave the Fe–O bond during the oxidation reaction. The energy separation between the d_{z^2} and d_{xy} (or d_{yz}) orbitals of **Int-p** is small, because the iron(Ⅱ) moiety has a weak interaction with the proximal oxygen atom transferred to the substrate. This situation allows a parallel-spin configuration to occur between the d_{z^2} and d_{xy} (or d_{yz}) orbitals. Thus, one up-spin electron is formally donated into the d_{z^2} orbital in the doublet state and the singly occupied d_{xy} (or d_{yz}) orbital in the quartet state is filled with a down-spin electron, resulting in the formation of the same electronic configuration in the heme porphyrin moiety in both spin states. On the other hand, the singly occupied $d_{x^2-y^2}$ orbital of the oxidant in the sextet spin state uptakes one electron from the π orbital of the substrate.

The assignment of the molecular orbital occupancy in Chart 2 is supported because the geometrical parameters of **Int-p** in the doublet and quartet states are similar, the Fe–O distances being 3.091 and 3.090 Å, the Fe–N bonds 2.036 and 2.035 Å, the Fe–S bonds 2.606 and 2.603 Å, respectively. This similarity in geometry is a consequence from the identical occupancy of the relevant orbitals of the heme porphyrin moiety in the doublet and quartet spin states. In contrast to this marked structural resemblance, the geometry of the sextet spin state is different from that of the doublet and quartet spin states. In particular, the sextet state has long Fe–N bonds of 2.121 Å in average, due to the occupation of the d_{xy} orbital which has an antibonding nature about the Fe–N bonds. In addition to the structural analysis, the spin densities shown in Table 3 document the chemical process well. As the reaction proceeds, the spin density on the iron atom changes as 1.0 → 1.8 → 2.0 in the doublet state, 2.6 → 2.4 → 2.0 in the quartet state, and 4.2 → 3.8 in the sextet state. The change in the spin density arises from the reduction of the iron atom from charge +3 to +2, resulting in the triplet electronic

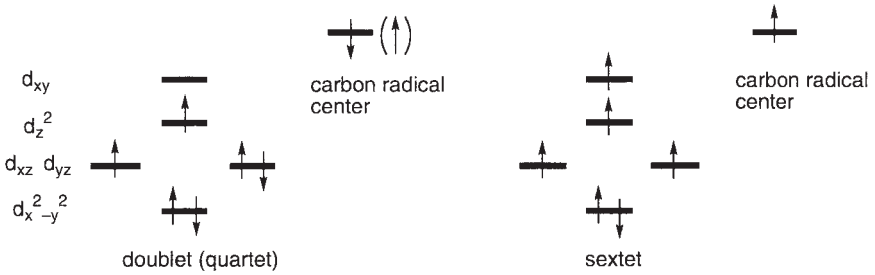

Chart 2.

Table 3. Calculated Mulliken Charges and Spin Densities for the Optimized Geometries in the Proximal Oxygen Transfer Mechanism (Values in Parentheses are Spin Densities)

	TS1-p		**Int-p**		
	Doublet	Quartet	Doublet	Quartet	Sextet
Fe	1.3 (1.8)	1.3 (2.4)	1.2 (2.0)	1.2 (2.0)	1.1 (3.8)
O (proximal)	−0.3 (−0.1)	−0.3 (0.1)	−0.3 (0.0)	−0.3 (0.1)	−0.3 (0.1)
O (distal)	−0.5 (0.0)	−0.5 (0.0)	−0.5 (0.0)	−0.5 (0.0)	−0.5 (0.0)
H[a)]	0.3 (0.0)	0.3 (0.0)	0.3 (0.0)	0.3 (0.0)	0.3 (0.0)
CH_3S	−0.5 (0.0)	−0.5 (0.2)	−0.6 (0.1)	−0.6 (0.2)	−0.5 (0.2)
Porphyrin	−1.3 (0.0)	−1.2 (−0.2)	−1.3 (−0.2)	−1.3 (−0.2)	−1.3 (0.0)
Substrate	0.0 (−0.7)	−0.1 (0.5)	0.2 (−0.9)	0.2 (0.9)	0.2 (0.9)

a) Hydrogen atom of 6th ligand of porphyrin.

configuration of the iron atom in the doublet and quartet states and the quintet configuration in the sextet state.

Clark and Hofmann calculated the oxirane-forming transition state that involves an O–O cleavage as well as a ring-closure process,[60a] although we did not calculate the corresponding transition state (**TS2-p**) in the proximal oxygen transfer mechanism. The barrier height for the transition state is 16 kcal/mol relative to the radical intermediate. If **Int-p** releases the oxidized substrate without any catalytic interaction with heme porphyrin, the activation energy for the second transition state in the proximal oxygen transfer mechanism is expected to be about 16 kcal/mol. Thus, the proximal oxygen transfer mechanism is unlikely to be responsible for olefin epoxidation by the iron(Ⅲ)–hydroperoxo species.

4. Distal Oxygen Transfer Mechanism. In the initial stages of this reaction, the O–O bond of the hydroperoxo moiety is dissociated and the distal oxygen atom is transferred to one of the carbon atoms of ethylene via **TS1-d**. In the resultant intermediate **Int-d**, the iron(Ⅳ)–oxo species retains a weak interaction with the hydroxy group of the oxidized substrate radical $^{\bullet}CH_2CH_2(OH)$. Transition state **TS1-d** has an imaginary frequency of 722i cm^{-1} due to O–O and C–O stretching. This is consistent with what we expect in the "distal oxygen transfer mechanism".

Figure 4 shows changes in the charge and spin densities along the reaction pathway from the iron(Ⅲ)–hydroperoxo species to **TS1-d**. The charge and spin densities in the Fe, porphyrin, and axial ligand moieties are almost unchanged, but a significant change from the homolytic cleavage of the O–O bond is seen in the substrate and the hydroperoxo moiety of the oxidant. The geometrical change is also small; the Fe–O bond changes from 2.004 to 1.913 Å, the Fe–S bond from 2.644 to 2.671 Å, the Fe–N bond from 2.093 to 2.098 Å. These computational results suggest that the iron atom of **TS1-d** remains in the oxidation state of +3, and that the orbital occupations in the iron, porphyrin ring, and proximal ligand moieties are not changed.

Chart 3 is an orbital representation of **Int-d**, by which we can look at the electronic and structural changes caused by the oxidation of the Fe atom from charge +3 to +4. What we see here is the configurational change from Chart 1 to Chart 3 via **TS1-d**. As discussed above, the d-block orbital of Fe on **TS1-d** has the same electron occupancy as that of the iron(Ⅲ)–hydroperoxo species. The oxidation of the Fe atom by the proximal oxygen atom occurs after the transition state to lead to the iron(Ⅳ)–oxo species. In the doublet pathway, a down-spin electron is released from the doubly occupied d_{xy} or d_{yz} orbital (indicated in Chart 1) and in the quartet pathway an up-spin electron is released from the singly occupied d_{z^2} orbital, resulting in the formation of an Fe=O double bond. Therefore **Int-d** in the doublet and quartet spin

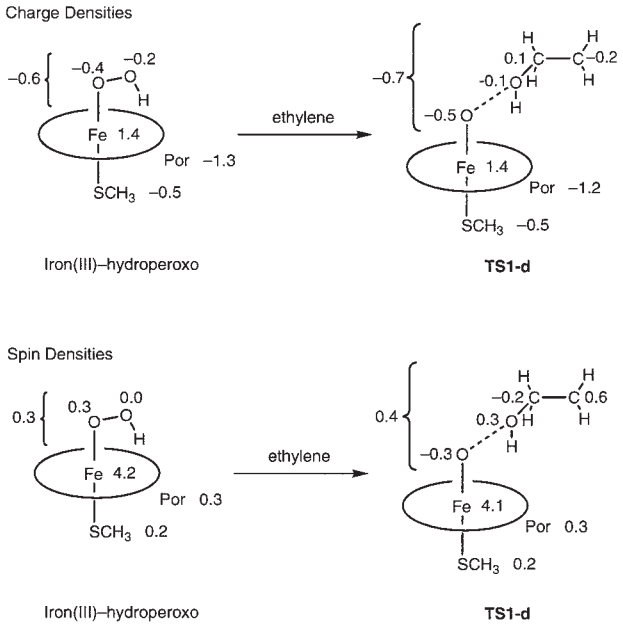

Fig. 4. Changes in charge and spin densities along the reaction pathway from iron(Ⅲ)–hydroperoxo species to **TS1-d**.

states possesses three unpaired electrons, two of which are localized in parallel in the FeO moiety while the third electron which determines its spin state exists on the terminal carbon radical center of the oxidized substrate (see Table 4). The unpaired electron on the terminal carbon atom has almost no magnetic interaction with the ferryl moiety, and as a result the doublet and quartet spin states of **Int-d** are close in energy. Therefore the geometries of **Int-d** in the doublet and quartet spin states are similar, due to the common electronic configuration and the weak interaction between the terminal CH_2 group and the FeO moiety.

On the other hand, the sextet state of **Int-d** has a different orbital occupancy, leading to different structural and electronic properties. In the sextet pathway, an up-spin electron is released from the singly occupied d_{z^2} orbital (indicated in Chart 1) to produce the iron(Ⅳ)–oxo species. Thus, **Int-d** in the sextet state has an unstable orbital occupancy, in which the d_{xy} orbital involving a strongly antibonding character in the Fe–N linkages is filled, as shown in Chart 3; thus **Int-d** is 7.6 kcal/mol higher in the sextet state than in the quartet state. The instability inevitably requires a spin-inversion process from the sextet to quartet spin state.[61] We successfully located **TS1-d** on the sextet potential energy surface, but all attempts to find the transition state on the

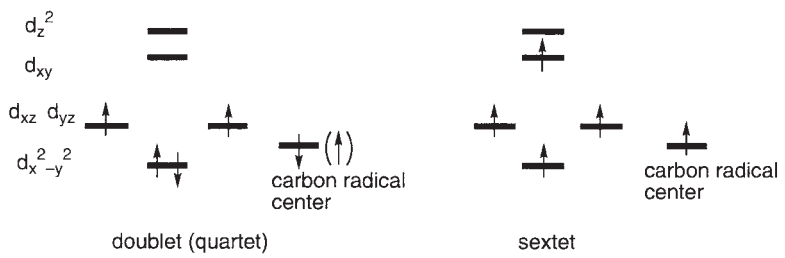

Chart 3.

Table 4. Calculated Mulliken Charges and Spin Densities for the Optimized Geomeries in the Distal Oxygen Transfer Mechanism (Values in Parentheses are Spin Densities)

	TS1-d	**Int-d**			**TS2-d**		Final complex	
	Sextet	Doublet	Quartet	Sextet	Doublet	Quartet	Doublet	Quartet
Fe	1.4 (4.1)	1.3 (1.4)	1.3 (1.4)	1.3 (3.4)	1.3 (1.3)	1.4 (2.4)	1.2 (1.0)	1.4 (2.7)
O (proximal)	−0.5 (−0.3)	−0.5 (0.7)	−0.5 (0.7)	−0.6 (0.5)	−0.7 (0.3)	−0.7 (0.3)	−0.7 (0.1)	−0.7 (0.2)
O (distal)	−0.5 (0.3)	−0.6 (−0.1)	−0.6 (0.1)	−0.6 (0.1)	−0.6 (0.1)	−0.6 (0.0)		
H[a)]	0.4 (0.0)	0.4 (0.0)	0.4 (0.0)	0.4 (0.0)	0.4 (0.0)	0.4 (0.0)	0.3 (0.0)	0.3 (0.0)
CH_3S	−0.5 (0.2)	−0.4 (0.0)	−0.4 (0.0)	−0.4 (−0.2)	−0.4 (0.0)	−0.4 (−0.1)	−0.4 (0.0)	−0.6 (0.2)
Porphyrin	−1.2 (0.3)	−1.2 (−0.1)	−1.2 (−0.1)	−1.1 (0.3)	−1.0 (−0.1)	−1.1 (−0.2)	−1.4 (−0.1)	−1.4 (−0.1)
Substrate	−0.1 (0.4)	0.0 (−0.9)	0.0 (0.9)	0.0 (0.9)	0.0 (−0.6)	0.0 (0.6)		

a) Hydrogen atom of 6th ligand of iron-hydroperoxo species.

doublet and quartet surfaces failed. We carried out restricted open-shell DFT (RO-DFT) calculations for **TS1-d** in the doublet and quartet states to rule out the spin-contamination problem in the spin-unrestricted calculations. However, this method also failed to locate the transition state and predicted that the doublet and quartet states lie more than 15 kcal/mol above the sextet state at the optimized structure of **TS1-d** in the sextet state. Thus, the sextet state is enegetically the most favorable.

The second half of the epoxidation reaction by the iron(Ⅲ)–hydroperoxo species is the ring-closure process. In contrast to the first half, we found the transition state for the ring-closure process in the doublet and quartet states. The optimized structure of **TS2-d** has an imaginary frequency mode that corresponds to a hydrogen atom abstraction as well as a ring closure; computed values in the doublet and quartet states are 870i and 535i cm^{-1}, respectively. The transition vector of **TS2-d** shown in Fig. 3 indicates the occurrence of epoxide ring closure and hydrogen atom transfer. In view of the imaginary mode, this transition state leads to the iron(Ⅲ)–hydroxo complex.

5. Is the Iron(Ⅲ)–Hydroperoxo Species a Powerful Oxidant ? It is interesting to look at how the electronic process of olefin epoxidation by the iron(Ⅲ)–hydroperoxo species is different from that by hydrogen peroxide itself. We performed additional calculations of ethylene epoxidation by hydrogen peroxide. The geometry and spin density distribution of the transition state is depicted in Fig. 5. The O–O bond of hydrogen peroxide is also cleaved homolytically in the course of the reaction, as confirmed from the spin density distribution of the transition state, 0.7 on the terminal carbon atom and −0.7 on the oxygen atom of the resultant hydroxyl radical. There is a close resemblance in geometry and spin density distribution between the chemical processes mediated by the iron(Ⅲ)–hydroperoxo species and by hydrogen peroxide. A computed activation energy of 22.4 kcal/mol for **TS1-d** is comparable to that for the transition state by hydrogen peroxide, 22.1 kcal/mol. This result fell short of our expectations. We must therefore conclude that the essential electronic features in the dissociation of the O–O bond and the formation of the C–O bond remain unchanged by the involvement of iron–porphyrin complex. In view of a well-known experimental fact that hydrogen peroxide is incapable of mediating olefin epoxidation, the iron(Ⅲ)–hydroperoxo species is unlikely to catalyze olefin epoxidation reactions.

In order to aid our understanding, we carried out DFT calculations at the same level of theory for ethylene epoxidation by a compound Ⅰ model with a CH_3S^- ligand. Shaik and

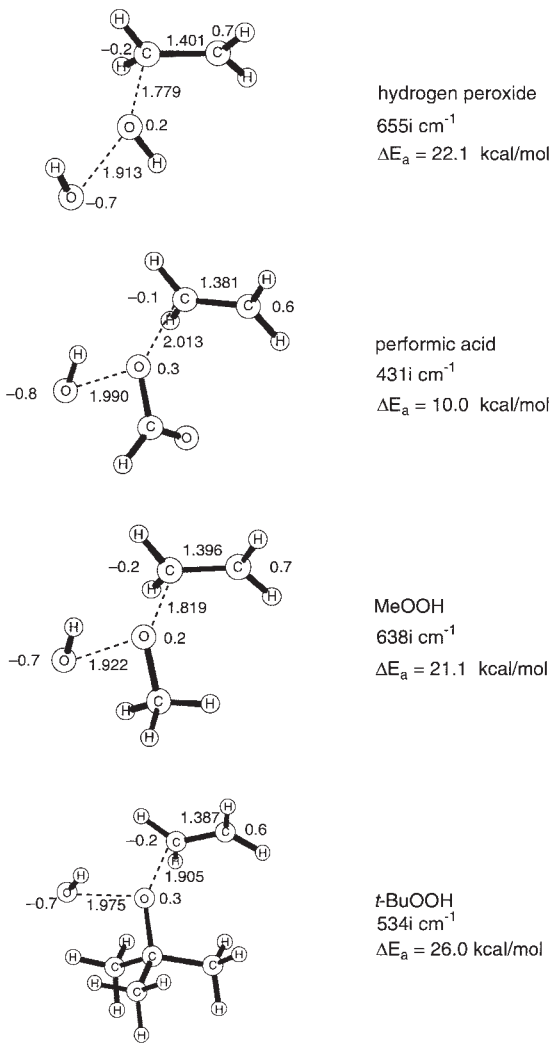

Fig. 5. Optimized geometries and spin density distributions of the transition states for ethylene epoxidation by hydrogen peroxide, performic acid, MeOOH, and *t*-BuOOH.

collaborators performed a detailed theoretical study of the reaction by an alternative model with an SH^- ligand in the doublet and quartet spin states, demonstrating that compound Ⅰ is a reasonable oxidant for this chemical process.[29] Computed energy diagrams and optimized geometries of the reaction species for the epoxidation of ethylene by our compound Ⅰ model are

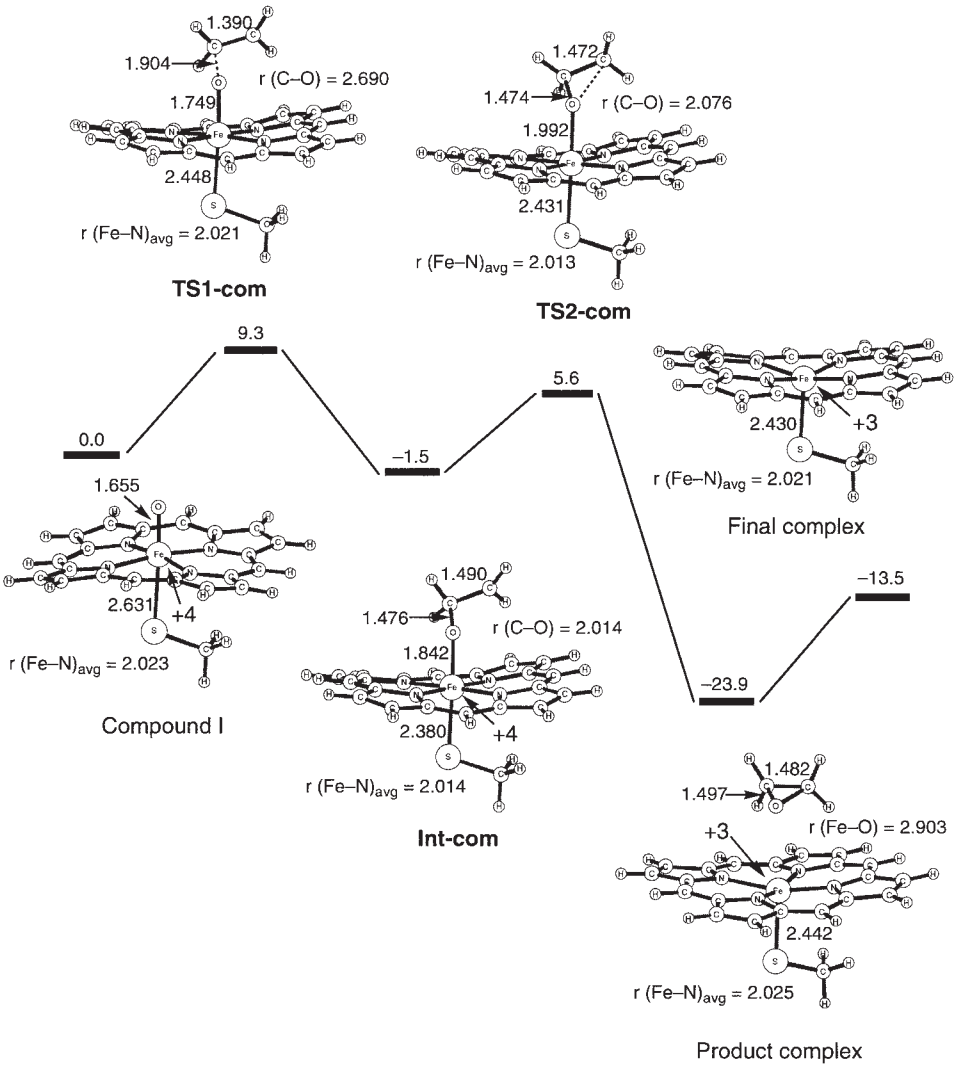

Fig. 6. Energy diagrams with optimized structures of the reaction species for ethylene epoxidation by a compound I model in the quartet state.

Table 5. Calculated Mulliken Charges and Spin Densities for the Optimized Geometries in Olefin Epoxidation by Compound I Model (Values in Parentheses are Spin Densities)

	Fe	O	CH_3S	Porphyrin	Substrate
Compound I	1.2 (1.2)	−0.4 (0.8)	−0.2 (0.4)	−0.6 (0.6)	
TS1-com	1.2 (1.2)	−0.5 (0.7)	0.0 (0.4)	−0.7 (0.2)	0.0 (0.5)
Int-com	1.3 (1.9)	−0.6 (0.3)	0.0 (0.0)	−0.8 (−0.1)	0.1 (0.9)
TS2-com	1.3 (2.4)	−0.5 (0.0)	−0.1 (0.2)	−1.0 (−0.3)	0.3 (0.7)
Product complex	1.2 (2.6)	−0.4 (0.0)	−0.2 (0.4)	−1.0 (0.0)	0.4 (0.0)
Final complex	1.1 (2.6)		−0.2 (0.4)	−0.9 (0.0)	

demonstrated in Fig. 6. The general profiles of the energies and the geometries are, of course, similar to those obtained in the previous study.[29] So our calculations do not add new information to the results of Shaik et al. concerning the mechanism of olefin epoxidation by compound I. Calculated charges and spin densities for the Fe and O atoms and the CH_3S and porphyrin moieties are listed in Table 5. These data characterize the electronic structures of the intermediates and transition states involved in olefin epoxidation by compound I. The formation of the covalent bond between the oxo ligand and a carbon atom of ethylene via **TS1-com** yields a radical complex, **Int-com**, which has an unpaired electron located on the terminal CH_2 group. The optimized structure of **TS1-com** is characterized by an imaginary frequency mode; the value in the quartet state is 549i cm^{-1}. The iron atom of **Int-com** still has charge +4 (the a_{2u} orbital of porphyrin heavily mixed with the p orbital of the sulfur ligand is filled), confirmed by the changes in the spin density along the reaction pathway. When we follow the potential energy diagram, the C–O bond formation should require 9.3 kcal/mol. The activation energy for the reaction is 13.1 kcal/mol lower than that

mediated by the iron(Ⅲ)–hydroperoxo species at the same level of theory. Therefore we conclude that olefin epoxidation should be mainly catalyzed by compound Ⅰ and that the iron(Ⅲ)–hydroperoxo species is unlikely to promote the reaction. The iron atom of the final complex shown in Fig. 6 is located 0.283 Å above the porphyrin ring, in line with known experimental data.[1a,1h]

The ring-closure transition state, **TS2-com**, that is shown in Fig. 6 has an imaginary frequency of 576i cm^{-1}. The activation energy for this transition state is 7.1 kcal/mol relative to **Int-com**. In contrast to **TS2-com**, **TS2-d** has a very high activation barrier of 19.9 kcal/mol. P450-catalyzed epoxidation of terminal olefins is paralleled, in many instances, by N-alkylation of the heme group and inactivation of the enzyme, which suggests the formation of a carbon radical or cation intermediate generated via a pathway that is either independent of or in competition with epoxide formation.[1h,62–64] Studies of the oxidation of terminal olefins by a model iron porphyrin system indicate that heme alkylation usually occurs less often than once in 300 turnovers. The terminal CH_2 group of **Int-d**, which has an unpaired electron, is more likely to be trapped by one of the pyrrole nitrogen atoms prior to the closure of the epoxide ring which has a high activation barrier.

In several experiments,[26,27] peracids and alkylhydroperoxides were used as oxidants for modeling P450-catalyzed reactions; we therefore calculated the transition states for ethylene epoxidation by performic acid, MeOOH, and *t*-BuOOH. We show in Fig. 5 optimized geometries and spin density distributions of the transition states. These are similar to the transition state for ethylene epoxidation by hydrogen peroxide in geometry and spin density distribution. A calculated activation energy for ethylene epoxidation by performic acid is 10.0 kcal/mol, this value being comparable to that obtained in the case of compound Ⅰ (9.3 kcal/mol). Since the mechanism and energetics of ethylene epoxidation remain unchanged by the involvement of iron-porphyrin complex, the activation energy for olefin epoxidation by the iron(Ⅲ)–formylperoxo species would remain unchanged from 10.0 kcal/mol. This result is in good agreement with the experimental observation that, under conditions lacking robust proton transport to the bound oxy species, the acylperoxo species should have an extended lifetime and play a role in olefin epoxidation.[26] The DFT calculations also predict that this reaction should occur. However, we do not think that the experiments[26,27] can reasonably support the involvement of the iron(Ⅲ)–hydroperoxo species in olefin epoxidation in vivo because the calculated activation energy is much lower than that for ethylene epoxidation by hydrogen peroxide, the reactivity of which is almost same as that of the actual iron–hydroperoxo species. In contrast to performic acid, ethylene epoxidation by MeOOH and *t*-BuOOH has barriers of 21.1 kcal/mol and 26.0 kcal/mol, respectively. This is comparable to that by hydrogen peroxide. Indeed, alkylperoxo species are experimentally reported to be unreactive to olefins.[26] These results clearly indicate that the iron–hydroperoxo species is not responsible for olefin epoxidation.

Conclusions

We have studied the mechanism and energetics for the epoxidation of ethylene by an iron(Ⅲ)–hydroperoxo model of P450 using B3LYP DFT calculations. There are two possible entrance channels in the reaction: a proximal oxygen transfer mechanism and a distal oxygen transfer mechanism. The proximal oxygen transfer mechanism is initiated by the homolytic cleavage of the Fe–O bond to form a radical intermediate involving $^{\bullet}CH_2CH_2(OOH)$. Since this radical intermediate is energetically unstable compared to another intermediate formed in the distal oxygen transfer mechanism, the transfer of the proximal oxygen atom to a carbon atom of ethylene is energetically unlikely. The distal oxygen transfer mechanism involves the homolytic cleavage of the O–O bond in the initial stages of the reaction, and the resultant iron(Ⅳ)–oxo complex retains a weak interaction with the hydroxy group of the radical intermediate involving $^{\bullet}CH_2CH_2(OH)$. The activation barrier for this process is rather high (22.4 kcal/mol relative to the dissociation limit on the sextet potential energy surface) and this oxidation process bears energetic, structural, and electronic resemblance to olefin epoxidation mediated by hydrogen peroxide, although it does not occur experimentally. These findings suggest that the essential electronic features in the dissociation of the O–O bond and the formation of the C–O bond remain unchanged by the involvement of the iron–porphyrin complex. We performed additional calculations for the epoxidation of ethylene by a compound Ⅰ model with an SCH_3 ligand. We concluded from the energetic point of view that olefin epoxidation should be mainly catalyzed by compound Ⅰ and that the iron–hydroperoxo species is unlikely to promote the reaction.

K.Y. acknowledges a Grant-in-Aid for Scientific Research on the Priority Area "Molecular Physical Chemistry" from the Ministry of Education, Science, Sports and Culture and the Iwatani Naoji Foundation's Research Grant for their support of this work. Computations were partly carried out at the Computer Center of the Institute for Molecular Science.

References

1 Reviews for example: a) M. Sono, M. P. Roach, E. D. Coulter, and J. H. Dawson, *Chem. Rev.*, **96**, 2841 (1996). b) B. Meunier, *Chem. Rev.*, **92**, 1411 (1992). c) M. Newcomb and P. H. Toy, *Acc. Chem. Res.*, **33**, 449 (2000). d) D. Dolphin, T. G. Traylor, and L. Y. Xie, *Acc. Chem. Res.*, **30**, 251 (1997). e) J. McLain, J. Lee, and J. T. Groves, in "Biomimetic Oxidations Catalyzed by Transition Metal Complexes," ed by B. Munier, Imperial College Press, London, (2000), pp. 91–169. f) H. Shimada, S. G. Sligar, H. Yeom, and Y. Ishimura, in "Oxygenases and Model Systems," ed by T. Funabiki, Kluwer Academic Publishers, Dordrecht, The Netherlands, (1997), pp. 195–221. g) Y. Watanabe, in "Oxygenases and Model Systems," ed by T. Funabiki, Kluwer Academic Publishers, Dordrecht, The Netherlands, (1997), pp. 223–282. h) "Cytochrome P-450: Structure, Mechanisms and Biochemistry," 2nd ed, ed by P. R. Oritz de Montellano, Plenum, New York, (1995). i) P. R. Ortiz de Montellano, *Acc. Chem. Res.*, **31**, 543 (1998).

2 a) M. Newcomb, M. H. Le Tadic, D. A. Putt, and P. F. Hollenberg, *J. Am. Chem. Soc.*, **117**, 3312 (1995). b) M. Newcomb, M. H. Le Tadic-Biadatti, D. L. Chestney, E. S. Roberts, and P. F. Hollenberg, *J. Am. Chem. Soc.*, **117**, 12085 (1995). c) P. H. Toy, M. Newcomb, and P. F. Hollenberg, *J. Am. Chem. Soc.*, **120**, 7719 (1998). d) J. K. Atkinson, P. F. Hollenberg, K. U. Ingold, C. C. Johnson, M.-H. Le Tadic, M. Newcomb, and D. A. Putt, *Biochemistry*, **33**, 10630 (1994). e) M. Newcomb, R. Shen, S.-Y.

Choi, P. H. Toy, P. F. Hollenberg, A. D. N. Vaz, and M. J. Coon, *J. Am. Chem. Soc.*, **122**, 2677 (2000).

3 R. Davydov, T. M. Makris, V. Kofman, D. E. Werst, S. G. Sligar, and B. M. Hoffman, *J. Am. Chem. Soc.*, **123**, 1403 (2001).

4 a) Z. Gross and S. Nimri, *J. Am. Chem. Soc.*, **117**, 8021 (1995). b) Z. Gross and S. Nimri, *Inorg. Chem.*, **33**, 1731 (1994).

5 J. T. Groves, Z. Gross, and M. K. Stern, *Inorg. Chem.*, **33**, 5065 (1994).

6 K. Czarnecki, S. Nimri, Z. Gross, L. M. Proniewicz, and J. R. Kincaid, *J. Am. Chem. Soc.*, **118**, 2929 (1996).

7 a) W. Nam, Y. M. Goh, Y. J. Lee, M. H. Lim, and C. Kim, *Inorg. Chem.*, **38**, 3238 (1999). b) Y. M. Goh and W. Nam, *Inorg. Chem.*, **38**, 914 (1999). c) S. J. Yang and W. Nam, *Inorg. Chem.*, **37**, 606 (1998). d) K. A. Lee and W. Nam, *J. Am. Chem. Soc.*, **119**, 1916 (1997).

8 W. Adam, V. R. Stegmann, and C. R. Saha-Möller, *J. Am. Chem. Soc.*, **121**, 1879 (1999).

9 P. R. Ortiz de Montellano, B. L. K. Mangold, C. Wheeler, K. L. Kunze, and N. O. Reich, *J. Biol. Chem.*, **258**, 4208 (1983).

10 R. E. White, J. P. Miller, L. V. Favreau, and A. Bhattacharyya, *J. Am. Chem. Soc.*, **108**, 6024 (1986).

11 T. G. Traylor, K. W. Hill, W.-P. Fann, S. Tsuchiya, and B. E. Dunlap, *J. Am. Chem. Soc.*, **114**, 1308 (1992).

12 A. Sorokin, A. Robert, and B. Meunier, *J. Am. Chem. Soc.*, **115**, 7293 (1993).

13 J. T. Groves, G. A. McClusky, R. E. White, and M. J. Coon, *Biochem. Biophys. Res. Commun.*, **81**, 154 (1978).

14 M. H. Gelb, D. C. Heimbrook, P. Mälkönen, and S. G. Sligar, *Biochemistry*, **21**, 370 (1982).

15 J. P. Jones, A. E. Rettie, and W. F. Trager, *J. Med. Chem.*, **33**, 1242 (1990).

16 J. T. Groves, R. C. Haushalter, M. Nakamura, T. E. Nemo, and B. J. Evans, *J. Am. Chem. Soc.*, **103**, 2884 (1981).

17 J. T. Groves, *J. Chem. Educ.*, **62**, 928 (1985).

18 J. Daly, *Handb. Exp. Pharmacol.*, **28**, 285 (1971).

19 D. Ostovic and T. C. Bruice, *Acc. Chem. Res.*, **25**, 314 (1992).

20 a) F. Ogliaro, N. Harris, S. Cohen, M. Filatov, S. P. de Visser, and S. Shaik, *J. Am. Chem. Soc.*, **122**, 8977 (2000). b) N. Harris, S. Cohen, M. Filatov, F. Ogliaro, and S. Shaik, *Angew. Chem., Int. Ed.*, **39**, 2003 (2000). c) M. Filatov, N. Harris, and S. Shaik, *Angew. Chem., Int. Ed.*, **38**, 3510 (1999).

21 a) K. Yoshizawa, Y. Kagawa, and Y. Shiota, *J. Phys. Chem. B*, **104**, 12365 (2000). b) K. Yoshizawa, T. Kamachi, and Y. Shiota, *J. Am. Chem. Soc.*, **123**, 9806 (2001).

22 M. Hata, Y. Hirano, T. Hoshino, and M. Tsuda, *J. Am. Chem. Soc.*, **123**, 6410 (2001).

23 I. Schlichting, J. Berendzen, K. Chu, A. M. Stock, S. A. Maves, D. E. Benson, R. M. Sweet, D. Ringe, G. A. Petsko, and S. G. Sligar, *Science*, **287**, 1615 (2000).

24 a) G. H. Loew and D. L. Harris, *Chem. Rev.*, **100**, 407 (2000). b) D. L. Harris and G. H. Loew, *J. Am. Chem. Soc.*, **120**, 8941 (1998).

25 a) A. D. N. Vaz, D. F. McGinnity, and M. J. Coon, *Proc. Natl. Acad. Sci. U.S.A.*, **95**, 3555 (1998). b) A. D. N. Vaz, S. J. Pernecky, G. M. Raner, and M. J. Coon, *Proc. Natl. Acad. Sci. U.S.A.*, **93**, 4644 (1996).

26 a) W. Nam, H. J. Han, S.-Y. Oh, Y. J. Lee, M.-H. Choi, S.-Y. Han, C. Kim, S. K. Woo, and W. Shin, *J. Am. Chem. Soc.*, **122**, 8677 (2000). b) W. Nam, M. H. Lim, H. J. Lee, and C. Kim, *J. Am. Chem. Soc.*, **122**, 6641 (2000). c) Y. J. Lee, Y. M. Goh, S.-Y. Han, C. Kim, and W. Nam, *Chem. Lett.*, **1998**, 837.

27 a) K. Machii, Y. Watanabe, and I. Morishima, *J. Am. Chem. Soc.*, **117**, 6691 (1995). b) Y. Watanabe, K. Yamaguchi, I. Morishima, K. Takehira, M. Shimizu, T. Hayakawa, and H. Orita, *Inorg. Chem.*, **30**, 2581 (1991).

28 a) M. F. Sisemore, M. Selke, J. N. Burstyn, and J. S. Valentine, *Inorg. Chem.*, **36**, 979 (1997). b) M. F. Sisemore, J. N. Burstyn, and J. S. Valentine, *Angew. Chem., Int. Ed. Engl.*, **35**, 206 (1996). c) M. Selke, M. F. Sisemore, and J. S. Valentine, *J. Am. Chem. Soc.*, **118**, 2008 (1996).

29 S. P. de Visser, F. Ogliaro, N. Harris, and S. Shaik, *J. Am. Chem. Soc.*, **123**, 3037 (2001).

30 A. D. Becke, *J. Chem. Phys.*, **98**, 5648 (1993).

31 A. D. Becke and M. R. Roussel, *Phys. Rev. A*, **39**, 3761 (1989).

32 C. Lee, W. Yang, and R. G. Parr, *Phys. Rev. B*, **37**, 785 (1988).

33 S. H. Vosko, L. Wilk, and M. Nusair, *Can. J. Chem.*, **58**, 1200 (1980).

34 a) W. J. Stevens, H. Basch, and M. Krauss, *J. Chem. Phys.*, **81**, 6026 (1984). b) W. J. Stevens, M. Krauss, H. Basch, and P. G. Jasien, *Can. J. Chem.*, **70**, 612 (1992).

35 a) R. Ditchfield, W. J. Hehre, and J. A. Pople, *J. Chem. Phys.*, **54**, 724 (1971). b) W. J. Hehre, R. Ditchfield, and J. A. Pople, *J. Chem. Phys.*, **54**, 2257 (1972).

36 W. J. Hehre, R. F. Stewart, and J. A. Pople, *J. Chem. Phys.*, **51**, 2657 (1969).

37 W. J. Hehre, R. Ditchfield, and J. A. Pople, *J. Chem. Phys.*, **56**, 2257 (1972).

38 To refine the energies, we carried out additional single-point calculations with the 6-31G(d) basis set for all atoms except Fe about the iron–hydroperoxo species and the transition states. The calculated activation energy remains almost unchanged.

39 M. J. Frisch, G. W. Trucks, H. B. Schlegel, G. E. Scuseria, M. A. Robb, J. R. Cheeseman, V. G. Zakrzewski, J. A. Montgomery, R. E. Stratmann, J. C. Burant, S. Dapprich, J. M. Millam, A. D. Daniels, K. N. Kudin, M. C. Strain, O. Farkas, J. Tomasi, V. Barone, M. Cossi, R. Cammi, B. Mennucci, C. Pomelli, C. Adamo, S. Clifford, J. Ochterski, G. A. Petersson, P. Y. Ayala, Q. Cui, K. Morokuma, D. K. Malick, A. D. Rabuck, K. Raghavachari, J. B. Foresman, J. Cioslowski, J. V. Ortiz, B. B. Stefanov, G. Liu, A. Liashenko, P. Piskorz, I. Komaromi, R. Gomperts, R. L. Martin, D. J. Fox, T. Keith, M. A. Al-Laham, C. Y. Peng, A. Nanayakkara, C. Gonzalez, M. Challacombe, P. M. W. Gill, B. G. Johnson, W. Chen, M. W. Wong, J. L. Andres, M. Head-Gordon, E. S. Replogle, and J. A. Pople, ''Gaussian 98,'' Gaussian Inc., Pittsburgh, PA (1998).

40 H. A. O. Hill, P. D. Skyte, J. W. Buchler, H. Lueken, M. Tonn, A. K. Gregson, and G. Pellizer, *J. Chem. Soc., Chem. Commun.*, **1979**, 151.

41 A. K. Gregson, *Inorg. Chem.*, **20**, 81 (1981).

42 D. L. Harris and G. H. Loew, *J. Am. Chem. Soc.*, **118**, 10588 (1996).

43 The proximal oxygen atom has some minor spin density because of the Fe(d)–O(p) admixture, which is not depicted in Chart 1 for simplicity.

44 J. Bernadou, A.-S. Fabiano, A. Robert, and B. Meunier, *J. Am. Chem. Soc.*, **116**, 9375 (1994).

45 J. Bernadou and B. Meunier, *Chem. Commun. (Cambridge, U.K.)*, **1998**, 2167.

46 O. Zakharieva, M. Grodzicki, A. X. Trautwein, C. Veeger, and I. M. C. M. Rietjens, *J. Biol. Inorg. Chem.*, **1**, 192 (1996).

47 J. Antony, M. Grodzicki, and A. X. Trautwein, *J. Phys. Chem. A*, **101**, 2692 (1997).

48 a) M. T. Green, *J. Am. Chem. Soc.*, **120**, 10772 (1998). b) M.

T. Green, *J. Am. Chem. Soc.*, **121**, 7939 (1999). c) M. T. Green, *J. Am. Chem. Soc.*, **122**, 9495 (2000).

49 a) F. Ogliaro, S. Cohen, S. P. de Visser, and S. Shaik, *J. Am. Chem. Soc.*, **122**, 12892 (2000). b) F. Ogliaro, S. P. de Visser, J. T. Groves, and S. Shaik, *Angew. Chem., Int. Ed.*, **40**, 2874 (2001).

50 T. Ohta, K. Matsuura, K. Yoshizawa, and I. Morishima, *J. Inorg. Biochem.*, **82**, 141 (2000).

51 C. Linde, B. Åkermark, P.-O. Norrby, and M. Svensson, *J. Am. Chem. Soc.*, **121**, 5083 (1999).

52 a) R. D. Bach, M. N. Glukhovtsev, and C. Gonzalez, *J. Am. Chem. Soc.*, **120**, 9902 (1998). b) R. D. Bach, C. Canepa, J. E. Winter, and P. E. Blanchette, *J. Org. Chem.*, **62**, 5191 (1997). c) R. D. Bach, A. L. Owensby, C. Gonzalez, H. B. Schlegel, and J. J. W. McDouall, *J. Am. Chem. Soc.*, **113**, 2338 (1991).

53 a) A. Armstrong, I. Washington, and K. N. Houk, *J. Am. Chem. Soc.*, **122**, 6297 (2000). b) K. N. Houk, J. Liu, N. C. DeMello, and K. R. Condroski, *J. Am. Chem. Soc.*, **119**, 10147 (1997).

54 S. Yamabe, C. Kondou, and T. Minato, *J. Org. Chem.*, **61**, 616 (1996).

55 V. G. Dryuk, *Tetrahedron*, **32**, 2855 (1976).

56 L. Cavallo and H. Jacobsen, *Angew. Chem., Int. Ed.*, **39**, 589 (2000).

57 F. A. Chavez and P. K. Mascharak, *Acc. Chem. Res.*, **33**, 539 (2000).

58 a) T. L. Allen, W. H. Fink, and D. H. Volman, *J. Phys. Chem.*, **100**, 5299 (1996). b) T. L. Allen, W. H. Fink, and D. H. Volman, *J. Photochem. Photobiol. A: Chem.*, **85**, 201 (1995).

59 G. M. Thurman and R. Steckler, *J. Phys. Chem. A*, **105**, 2192 (2001).

60 a) T. Clark and H. Hofmann, *J. Phys. Chem.*, **98**, 13797 (1994). b) H. Hofmann and T. Clark, *J. Am. Chem. Soc.*, **113**, 2422 (1991).

61 Spin inversion does not pose a problem since efficient changes of spin states and the presence of spin equilibria are well documented for iron porphyrins. See Refs. 19 and 40.

62 a) J. P. Collman, P. D. Hampton, and J. I. Brauman, *J. Am. Chem. Soc.*, **112**, 2977 (1990). b) J. P. Collman, P. D. Hampton, and J. I. Brauman, *J. Am. Chem. Soc.*, **112**, 2986 (1990).

63 K. L. Kunze, B. L. K. Mangold, C. Wheeler, H. S. Beilan, and P. R. Ortiz de Montellano, *J. Biol. Chem.*, **258**, 4202 (1983).

64 S. P. de Visser, F. Ogliaro, and S. Shaik, *Angew. Chem., Int. Ed.*, **40**, 2871 (2001).